N+CPT clock resonance

M. Crescimanno[1,*] and M. Hohensee[2]

[1]*Department of Physics and Astronomy, Youngstown State University, Youngstown, Ohio 44555, USA*
[2]*MS-59, Harvard-Smithsonian Center for Astrophysics, 60 Garden St., Cambridge, Massachusetts 02138, USA*
**Corresponding author: mcrescim@cc.ysu.edu*

Received June 30, 2008; revised October 6, 2008; accepted October 7, 2008;
posted October 13, 2008 (Doc. ID 98082); published November 26, 2008

In a typical compact atomic time standard a current modulated semiconductor laser is used to create the optical fields that interrogate the atomic hyperfine transition. A pair of optical sidebands created by modulating the diode laser become the coherent population trapping (CPT) fields. At the same time, other pairs of optical sidebands may contribute to other multiphoton resonances, such as three-photon *N*-resonance [Phys. Rev. A **65**, 043817 (2002)]. We analyze the resulting joint CPT and *N*-resonance (hereafter *N*+CPT) analytically and numerically. Analytically we solve a four-level quantum optics model for this joint resonance and perturbatively include the leading ac Stark effects from the five largest optical fields in the laser's modulation comb. Numerically we use a truncated Floquet solving routine that first symbolically develops the optical Bloch equations to a prescribed order of perturbation theory before evaluating. This numerical approach has, as input, the complete physical details of the first two excited-state manifolds of ^{87}Rb. We test these theoretical approaches with experiments by characterizing the optimal clock operating regimes.

OCIS codes: 020.1670, 020.3690, 120.3930, 300.6380.

1. INTRODUCTION

Coherent population trapping (CPT) [1] is a promising technique for small atomic time standards [2–7]. Very small CPT clocks may be made, in part because no direct microwave excitation of the atoms is necessary, as would be the case in a more traditional intensity optically pumped clock. Presently observed instability levels are significantly larger than ideal expectations, however, with some studies tracing the dominant contribution to the clock instability to laser phase and rf sideband noise [8–12].

In miniature CPT clocks [6] a diode laser is typically current modulated at half the hyperfine frequency; the resultant light fields are circularly polarized and tuned so that the carrier's frequency is the average of two ground-state hyperfine levels' optical excitation frequencies [Fig. 1(a)]. When the first sidebands are resonant with their respective hyperfine levels CPT increases the transparency of the atomic vapor, providing a marker for guiding the frequency of the modulation source [3,5]. One of the main reasons for using the first sidebands of a half-hyperfine frequency modulated laser is that the two interrogating laser fields are nearly the same intensity. Doing so minimizes the sensitivity of the CPT resonance to variations in the laser's detuning and intensity and also maximizes its visibility and symmetry [13]. Resonance line asymmetries contribute to instabilities in the output frequency [14,15]. There have also been many experimental and theoretical studies of the effect of laser diode current modulation depth [2,13,16,17] on clock performance.

Of late there has been experimental work regarding a three-photon resonance [18], called the *N*-resonance [see Fig. 1(b)] as an alternative to CPT techniques. For the *N*-resonance clock, optical pumping due to a nearly resonant field Ω_1 is frustrated by an off-resonant field Ω_0, which stimulates a two-photon Raman transition. This scheme can be implemented with a modulated laser diode by detuning the diode's center frequency one hyperfine interval from a ground-state optical transition. An *N*-resonance clock using a single external cavity laser diode and an electro-optic modulator (EOM) [19–21] has been built and tested with preliminary measurements indicating stability typical of laser-based CPT clocks. New experiments are presently under way to determine a rigorous Allan variance of a VCSEL-based *N*-resonance clock [22]. Interest in the use of *N*-resonances for clock applications is due to the superior contrast that they exhibit on the D_2 line of Rb as compared to CPT resonances on the same transition and because the *N*-resonance contrast does not degrade with increased buffer-gas pressure the way CPT resonances do [19,20]. This latter property makes the *N*-resonance particularly attractive for use as a chip-scale atomic frequency reference, where small interaction volumes require the buffer-gas pressure to be high. Additionally, there have been some indications that light shift cancellation is also possible in *N*-resonance clocks [21]. As we will show here, achieving full light shift compensation for *N*-resonance clocks is somewhat complicated by the effects of competing CPT processes, which are difficult to avoid in clocks using modulated lasers.

Whether one creates the nearly resonant sideband with an EOM or by modulating the laser diode's current, there will necessarily be additional resonant fields present. For example in Fig. 1(b), the laser diode would be red-detuned by one hyperfine interval from the lowest optical resonance so that the modulation that creates the Ω_1 field must also generate a second near-resonant sideband Ω_2. This second sideband, though small, cannot be ignored since it participates in a CPT resonance. Our model and experiments together indicate that even the transmission

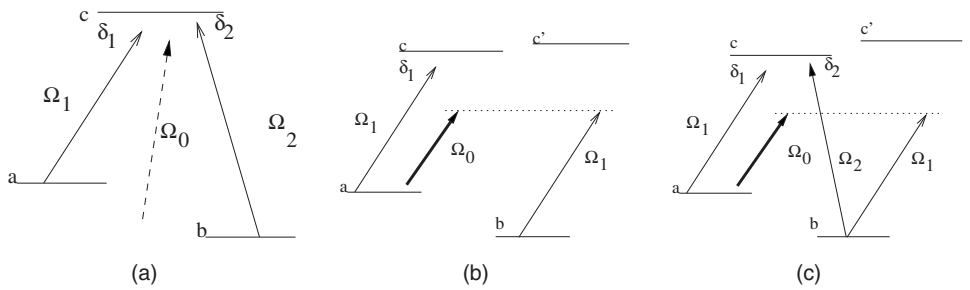

Fig. 1. (a) Basic three-level schematic in two nearly resonant light fields Ω_1 and Ω_2 for the CPT system and (b) basic N-resonance system. Note the off-resonant drive field Ω_0. The nonresonant polarizability of the atom as a whole receives contributions from many levels, their collective effect being rendered in terms of a single pseudolevel c'. (c) Combined N+CPT resonance system.

of just the first sideband Ω_1 alone is modified by the second sideband. For the joint N+CPT resonance, our model indicates that the optical conductance depends on the amplitude (and not the intensity) of the other near-resonant light field.

In the analytic work that follows, we will use a four-level model of the N+CPT resonance exhibited by the minimal three-level system. This approximation is justified by inspection of the leading order terms in the Fourier-space representation (i.e., the Floquet expansion) of the time-dependent equations of motion for the three-level system driven by Ω_0, Ω_1, and Ω_2. These equations prove to be dual to the Fourier-transform of the time-independent equations that result from the use of our four-level model.

In Section 2 we explain the key theoretical assumptions and technical ingredients in our four-level quantum optics model of the N+CPT resonance. Its analytical solution is a perturbative evaluation of the steady-state solution to the optical Bloch equations (OBEs) of the atom in a five beam cw laser field approximating a VCSEL's modulation comb. The solution leads to unwieldy analytical expressions, so we evaluate them numerically to compare with other models and to the experiment. Although the model allows us to phase each optical field separately, we have throughout this paper assumed for simplicity that the phases of the optical fields in the modulation comb are those of pure phase modulation. In Section 3 we describe a hybrid symbolic-numerical code, the truncated Floquet solver (TFS), that generates and solves the truncated Floquet expansion of the OBE. In contrast to our analytic result, which calculates higher order corrections to the solution due to the ac Stark effect, the numerical code yields solutions approximate in the coupling between the relevant density matrix Fourier components and can calculate them in any configuration or phase of applied fields.

In Section 4 we compare both the analytic solution (of the simplified four-level system) and the numerical TFS to basic experimental phenomenology of the joint resonance. The utility of a theoretical model for clock applications is mainly used in locating and comparing optimal clock operating regimes. For example suppose that the clock's frequency is determined solely by that of the resonance's transmission extremum. Our theory locates operational set points at which changes in the laser's center frequency and power do not (in leading order) alter the frequency of the transmission extremum. Some of these set points have been found by exhaustive experimental investigations [19–21,23] directed by earlier theoretical work [24].

2. FOUR-LEVEL QUANTUM OPTICS MODEL OF THE JOINT COHERENT POPULATION TRAPPING AND *N*-RESONANCE

The simplified four-level quantum optics model of Fig. 1(c) is solved to leading order by adiabatically eliminating the nonresonant state c' from the OBEs. The N-resonance is a result of a two-photon lambda system in Ω_0 and Ω_1 impeding optical pumping to state b caused by Ω_1 alone. The key physical input is that the carrier, Ω_0, excites off-resonant polarization that couples with Ω_1 resulting in polarization and population redistribution of the ground state.

A three-level system is not (in general) sufficient to account for all the off-resonant polarizability that contributes to this process in a real atom. The simplest quantum optics model of the N-resonance includes a nonresonant c' state that has nonzero dipole matrix elements to the states a and b (here hyperfine groundstates). The state c' is a representative for all the states of the atom that contribute to the atom's off-resonant polarizability (not exclusively in the drive field Ω_0). Thus the ersatz level c' in our model is not a particular atomic level in the rubidium atom *per se*, but its position and couplings are chosen to reproduce the net contribution from all states having nonzero dipole matrix elements with ground states a (and b). This is distinct from what is commonly understood as the ac Stark effect, which refers to nonresonant polarizability in states already included in the Λ system. The main physical insight that the solution of this simplified quantum optics model provides is a detailed account of the interference between the N and CPT resonances, and this is most clearly displayed by the evolution equation for the ground-state coherence, ρ_{ab}.

For simplicity, we ignore throughout this entire paper propagation effects in the cell. These effects could be profound at high optical depth, though most of the experiments to date have not operated in such a regime. In some experiments the optical pumping to trap states in a real vapor cell would effectively change the optical depth on the transition(s) in our four-level model. The TFS numerical model in Section 3 includes optical pumping effects, where this section's analytical solution does not.

Throughout this paper as in a typical clock application, we assume that a weak longitudinal magnetic field is applied, isolating the two-photon resonance of the hyperfine $m=0$ pair from those of the $m\neq 0$ states. Our model also ignores lateral diffusion of coherence and any effects of the particular buffer-gas or vapor cell geometry other than those that can be encoded into linear transport coefficients in our quantum optics model (for discussion of these effects see [25]). Finally, in the numerical evaluation of this analytic solution we have included an integration over the Boltzmann distribution of the one-photon detuning and a separate integration over the Lamb–Dicke kernel of the two-photon detunings. The latter includes effects due to the longitudinal diffusion of the coherence.

In N-resonance, an off-resonant field (Ω_0) modulates the transmission of resonant light fields Ω_1 (and Ω_2) by creating a polarization that scatters them. This scattering depends on two things: the magnitude of the off-resonant polarization due to Ω_0 and the two-photon detuning of the far (one-photon) detuned CPT system of Ω_1 and Ω_0. We solve the Bloch equation $\partial_t\rho=-i[H,\rho]+\mathcal{L}\rho$ of Fig. 1(c) that, written in the laboratory frame, arises from

$$H=\begin{bmatrix} E & \tilde{\Omega}_1(t) & 0 & \Omega_2(t) \\ \tilde{\Omega}_1(t) & h & \Omega_0(t) & 0 \\ 0 & \Omega_0(t) & e & \Omega_1(t) \\ \Omega_2(t) & 0 & \Omega_1(t) & 0 \end{bmatrix}, \tag{1}$$

$$\mathcal{L}\rho=\begin{bmatrix} -\gamma\rho_{cc} & -\gamma_2\rho_{ca} & 0 & -\gamma_2\rho_{cb} \\ -\gamma_2\rho_{ac} & \frac{\gamma}{2}\rho_{cc}-\Gamma_1(\rho_{aa}-\rho_{bb}) & 0 & -\Gamma\rho_{ab} \\ 0 & 0 & 0 & 0 \\ -\gamma_2\rho_{bc} & -\Gamma\rho_{ba} & 0 & \frac{\gamma}{2}\rho_{cc}+\Gamma_1(\rho_{aa}-\rho_{bb}) \end{bmatrix}, \tag{2}$$

where the orders of the rows correspond to states c, a, c', and b, respectively. Though associated with the same laser field, our treatment distinguishes $\tilde{\Omega}_1$ from Ω_1 to account for the possible differences in Clebsch–Gordan coefficients of the states they connect (here a-c and b-c', respectively).

Note that we have not included any phenomenological damping coefficients for the state c' because the leading terms in the perturbative evaluation of the Bloch equations do not depend strongly on these particular linear transport coefficients. These additional rates are included in the TFS analysis described in Section 3, and we ignore them in the analytical work below as they are significant primarily at high intensity or large one-photon detunings.

Let ω_1, ω_2, and ω_0 represent the frequencies of the Ω_1, Ω_2, and Ω_0 optical fields, respectively. In general there is no single rotating frame in which the system is time-independent, because in the lab frame, the CPT ground-state coherence oscillates at $\omega_2-\omega_1$ while for the N-resonance this coherence oscillates at $2\omega_1-\omega_0$. If, however, the fields are part of a single modulation comb (for simplicity, think of Ω_0, Ω_1, and Ω_2 as adjacent comb teeth), these two-photon detunings are just the modulation frequency or a small integer multiple of it. Thus, for the case of fields generated by a modulation comb, there is a rotating frame that dramatically simplifies our analysis.

It is useful to define one- and two-photon detunings of this comb relative to the atomic structure. For historical reasons we register our detuning in relation to the CPT condition, that is, we define $\delta_1=\omega_1-E+h$ and $\delta_2=\omega_2-E$, which leads to the natural definition of the one-photon detuning $\Delta=(\delta_1+\delta_2)/2=(\omega_1+\omega_2+h)/2-E$ and two-photon detuning $\delta=\delta_1-\delta_2=\omega_1-\omega_2+h$.

To the OBE using Eqs. (1) and (2), we apply the typical "clocklike" hierarchy in which $\delta,\Gamma,\Gamma_1,\Omega_i^2/h<\Omega_j<\Delta,\gamma,\gamma_1,h,e-E$ with $i,j=0,\pm 1,\pm 2$ only. With this in mind, define $h'=h+e-E$ and note that the OBE for the $\rho_{ic'}$ with $i=a,b,c$ components has in the rotating frame the coefficients $E-e-\omega_1+\omega_0\sim -h'$, $h-e+\omega_0\sim\Delta-h'$, and $-e+\omega_1\sim\Delta-h'$ and are thus large. We then solve these using the rotating wave approximation (RWA) to find

$$\rho_{cc'}=\frac{-1}{2h'}[\Omega_0\rho_{ca}+\Omega_1\rho_{cb}], \tag{3}$$

$$\rho_{ac'}=\frac{-1}{2(h'-\Delta)}[\Omega_0\rho_{aa}+\Omega_1\rho_{ab}], \tag{4}$$

$$\rho_{bc'}=\frac{-1}{2(h'-\Delta)}[\Omega_0\rho_{ba}+\Omega_1\rho_{bb}]. \tag{5}$$

Note that to this order there are no terms proportional to Ω_2.

Using Eqs. (3)–(5) to eliminate $\rho_{ac'}$, $\rho_{bc'}$ from the OBE, one finds

$$\left(-i\delta+\Gamma+i\frac{|\Omega_1|^2-|\Omega_0|^2}{h'-\Delta}\right)\rho_{ab}=-i\tilde{\Omega}_1^*\rho_{cb}+i\Omega_2\rho_{ac}+i\frac{\Omega_1\Omega_0}{h'-\Delta}(\rho_{bb}-\rho_{aa}). \tag{6}$$

The first two terms on the right-hand side (RHS) of Eq.

(6) drive the CPT resonance and the last term generates the N-resonance. The equation for the ground-state population difference $2d=\rho_{aa}-\rho_{bb}$ is similar to Eq. (6). Since the ground-state coherence ρ_{ab} contributes to the two-photon resonance, the interference between the CPT and N-resonance driving terms leads to novel features in the joint resonance that may allow for new ways to control clock instability. From the point of view of just one of the optical fields, say Ω_1, the N-resonance is absorptive, whereas CPT results in transparency. For reasons that we will discuss later (differential ac Stark shifts), the CPT and N-resonances will not in general be concentric. This implies that the joint two-photon resonance will in general have pronounced asymmetry, a phenomenon characterizing experimental findings [19,23] and further elucidated in this theory model [26].

Our model's computed location of the local maxima (absorption) and minima (transparency) of the two-photon optical response is graphed in Fig. 2. The graph was computed assuming parameters for ^{87}Rb vapor in a 30 torr Ne buffer-gas cell with illumination on the D_1 lines and a one-photon detuning of about +100 MHz. The ground state decoherence width was taken to be 100 Hz, and the first sideband Ω_1 was held fixed at 300 kHz throughout. Note that the ordinate is the log of the ratio of the Rabi frequencies Ω_0/Ω_2; thus total light intensity increases in both directions from the center of the graph. This means that to the right the character of the resonance is predominantly N whereas on the left it is predominantly CPT. The graph shows that this theory model contains pure CPT and pure N-resonance limiting cases, indicates power broadening, and overall its behavior is reminiscent of an avoided crossing.

3. TRUNCATED FLOQUET SOLVER

Analytically determining the steady-state response of an atomic system being driven by multiple fields, each of which may drive several transitions, is a challenging problem. Models derived from a near-resonant subset of the full set of states can significantly reduce the complexity of the overall problem as we have already shown. Such models can usually be constructed to capture much of the physics of the overall system but must rely upon separately calculated or measured input parameters to account for contributions from the rest of the atomic system. Numerical methods are a useful adjunct to analytic approaches since, in general, more of the system can be treated rigorously.

We have used a suite of programs, implemented in MATLAB, which can numerically solve the density matrix equations of motion (the OBE) for any quantum system. Such systems are specified by a set of interaction-free energy eigenstates, a set of transition amplitudes that can contribute to an interaction Hamiltonian, along with any additional set of external couplings, such as to a magnetic field, or to non-Hermitian terms representing the trace over couplings to an external reservoir. This library can be used to generate and solve both the time-dependent evolution and steady-state solution for the density matrix, the latter relying upon the TFS. The TFS iteratively generates the frequency-space Floquet expansion of the density matrix equations of motion. The particular expansion used here is also known as a Bloch expansion as it is used to find the steady-state (transform variable $\omega=0$) solution. Such techniques have previously been used in the solution of time-periodic Schrödinger equations [27], to calculate atomic energy spectra [28], and coherent scattering properties of atoms and molecules in strong periodic external fields, as well as in solid-state applications [29,30].

At each step, the TFS determines the Fourier-transformed interaction representation Lindblad equations of motion for a given set S of density matrix element Fourier components. For a quantum system with Hamiltonian $H=H_0+H_I$, with H_0 as the bare Hamiltonian, and

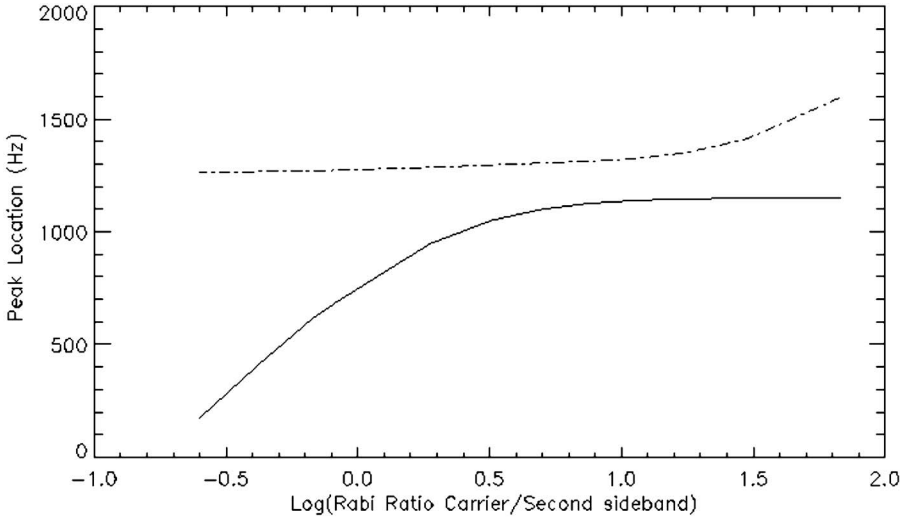

Fig. 2. Graph of the computed locations of the local maximum (dark curve) and minimum (dotted curve) of the two-photon optical response as a function of the ratio of the carrier to the second sideband Rabi frequencies. The motion of the two extrema is entirely a consequence of the activity of the fourth level combined with the ac Stark shift.

H_I as the interaction with the driving optical fields, magnetic fields, and other perturbative couplings, such equations take the form

$$-i\omega\tilde{\rho}_{jk}(\omega) = \frac{i}{\hbar}C[\rho_{jk}](\omega) + \sum_{j',k'} \mathcal{L}_{j'k',jk}\tilde{\rho}_{j'k'}(\omega), \tag{7}$$

where the first term on the RHS of Eq. (7) is

$$C[\rho_{jk}](\omega) = \int_{-\infty}^{\infty} dt e^{i\omega t}[\mathcal{H}_I(t), \rho_{jk}], \tag{8}$$

with $\mathcal{H}_I(t) = e^{iH_0 t} H_I e^{-iH_0 t}$. The second term of Eq. (7) accounts for incoherent relaxation processes associated with taking the trace over the system's couplings to an external reservoir [as $\mathcal{L}_\rho$ of Eq. (2)]. The Floquet expansion is obtained by first calculating the Fourier-transformed equations of motion for the full set of dc population terms ($\tilde{\rho}_{jj}(0)$) and is iteratively constructed by appending the Fourier-transformed equations for any new $\tilde{\rho}_{jk}(\omega)$ terms that appear. This generates a linear system of equations with the form $\mathbf{A}x = 0$, which in turn becomes $\mathbf{A}'x = b$ after the constraint $\Sigma_j \rho_{jj}(t) = 1$ is applied.

Although the matrix $\mathbf{A}$ used for our numerical solution of the N+CPT system is complicated (see Fig. 3), its most important properties are reflected in $\mathbf{A}$ for a simple two-level system. For the simplest nontrivial system involving only one transition between states $|a\rangle$ and $|b\rangle$, driven by two monochromatic fields whose frequencies differ by Δ, $\mathbf{A}$ has the form

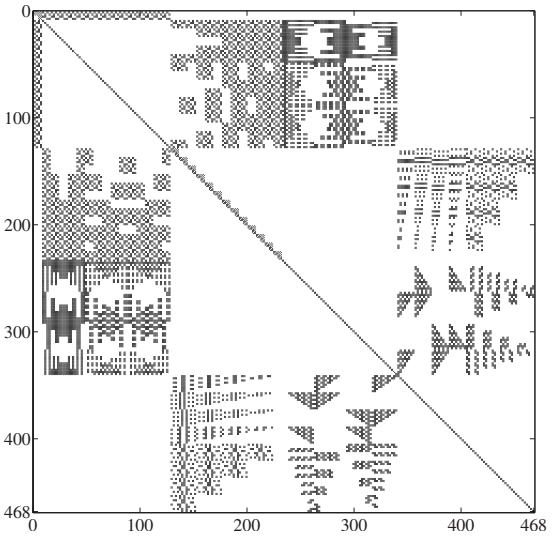

Fig. 3. Representation of the $\mathbf{A}$ matrix corresponding to a 15-field, four-level N+CPT resonance system. Dots correspond to nonzero matrix elements. This configuration is used to model the response of the four-level system to a doubly phased modulated laser, including the carrier Ω_0, the $\Omega_{\pm 1}$, and $\Omega_{\pm 2}$ fast modulation (at frequency $\sim h$) sidebands, and a pair of ± 1 slow modulation sidebands, to model the behavior of the clock lock. To improve numerical stability, our code solves the real and imaginary parts of each term in the Floquet expansion separately. Thus the size of this matrix is actually double the number of terms in the Floquet expansion.

$$\mathbf{A} = \begin{bmatrix} \ddots & & & & & & \\ & a_0 & b & & & & \\ & b^T & c_0 & d & & & \\ & & d^T & a_1 & b & & \\ & & & b^T & c_1 & d & \\ & & & & d^T & a_2 & \\ & & & & & & \ddots \end{bmatrix}, \tag{9}$$

where the submatrices $a_n = a_0$ and $c_n = c_0$, except for a constant imaginary shift of the diagonals: $a_n^{ij} = a_0^{ij} + n\Delta$ and $c_n^{ij} = c_0^{ij} + n\Delta$. More concretely, the coherence between the two states established by and coupled to the first field is $\tilde{\rho}_{ab}(\omega_1)$. This coherence couples not only to the $\tilde{\rho}_{aa}(0)$ and $\tilde{\rho}_{bb}(0)$ terms but also to $\tilde{\rho}_{aa}(\Delta)$ and $\tilde{\rho}_{bb}(\Delta)$ due to the interaction with the second field. These ac population components couple to higher harmonic Fourier components of $\tilde{\rho}_{ab}$, which in turn couple to more ac populations, and so on. The self-coupling for each term in the Floquet expansion is of the form $-\Gamma + i(\omega + n\Delta)$, so as the expansion proceeds, the magnitude of each new term is typically reduced due to dampening and dephasing relative to the driving terms closer to the dc populations. Provided that either the decoherence rate Γ of the ρ_{ab} or the detuning Δ is sufficiently large compared to the Rabi frequencies Ω_j of the applied fields, the contribution of the virtual states and coherences to the dc-coupled optical coherences rapidly converges to zero, and thus the system's solution is well approximated by that of the truncated Floquet expansion. For more complicated quantum systems, the shift of the diagonal elements of $\mathbf{A}$ from one n to the next can vary according to the particular coupling of each coherence to the applied fields, and some care must be taken to ensure these shifts are not too small, both for numerical stability and to ensure that the system converges for a reasonably sized Floquet expansion.

The best criteria for determining the truncation level varies from system to system and sometimes according to the chosen range of parameters. For the purposes of this paper, we chose to work in the unsaturated limit, ensuring that for any term driven by a set of fields with amplitudes Ω_j, either Ω_j/Γ or Ω_j/h is a small parameter. When solving the reduced (by conservation of total population) matrix equations, the only Floquet elements whose equations contain a source term are those directly coupled to the dc populations. We therefore determine the significance of a given term in the Floquet expansion on the basis of the degree to which it is driven by such source terms.

The network of couplings between each of the terms in the density matrix's Floquet expansion can be represented as an undirected graph. Using this representation, we assign each term in the Floquet expansion an "order" in each of the applied fields, where for each field, a term's order is equal to the minimum number of couplings mediated by that field along a path from the term to a term representing a dc population component. The order in the fields of a given term is equal to the number of photons each field contributes toward the virtual process that drives that term. Incoherent of dc couplings do not count toward a term's order. Terms whose order exceeds some

chosen threshold are approximated as zero, truncating the Floquet expansion. In our analytic approach, we apply perturbative corrections to a leading order solution of the optical polarization responsible for the $N+$CPT resonance. In contrast, the truncated Floquet expansion provides solutions that are perturbative in the couplings between that polarization and other terms in the atomic density matrix.

4. EXPERIMENTAL CONSEQUENCES

For any frequency standard based on the $N+$CPT resonance it is useful to find an operational regime in which the nominal clock frequency (which for discussion purposes in this section we take to be the local extremum of the optical response) is independent in linear order to wander in the laser frequency and intensity. For example, the CPT configuration (only two optical fields) has an optimal operating regime at $\Omega_1=\Omega_2$ and zero one-photon detuning [2]. When other optical fields are present (as is the case in the light from a current modulated laser diode), although the other fields cause ac Stark effects, it is often possible to find optimal modulation parameters for which the resulting two-photon line center is again independent (to leading order) of laser fequency and intensity variations (see [17]) and one-photon detunings. Similarly, for the N-resonance a different optimal operating configuration can be found [19–24] experimentally. We now approximate the analytical theory model of Section 1 to derive a simple closed-form expression for the optimal operating point of a joint $N+$CPT resonance-based clock.

To simplify the analytical solution of the four-level system, we study the limit in which the population in the excited state remains negligible, $\rho_{c'c'}=\rho_{cc}=0$. Let $2d=\rho_{aa}-\rho_{bb}$ represent the ground-state population difference, and so ρ_{aa}, $\rho_{bb}=\frac{1}{2}\pm d$, respectively (in this section of the report only). Furthermore, to simplify the equations and approach the parameter range in the experiment, we are interested in expanding the solution to the model to lowest (here first) order in the Ω_2. We are most interested in the δ (two-photon detuning) dependence of the optical response in the Ω_1 field only,

$$\begin{aligned}\text{Optical Response} &= -i(\Omega_1\rho_{bc'}+\tilde{\Omega}_1\rho_{ac})+c.c.\\ &= -i\frac{\Omega_0\Omega_1\rho_{ba}}{h-\Delta}+i\Omega_1\rho_{ac}+c.c..\end{aligned} \quad (10)$$

Clearly to the leading order in the Ω_2 field, the last term has a more modest dependence on δ than the first, proportional to the imaginary part of ρ_{ab}. In this section we take all the optical fields Ω_i, $i=0,1,2$ to be real and take the other sidebands not in Fig. 1(c) to be zero. Using Eq. (6) we have

$$F\rho_{ab}=-\frac{i\Omega_1\Omega_0}{(h-\Delta)}d-i\tilde{\Omega}_1^*\rho_{cb}+i\Omega_2\rho_{ac}, \quad (11)$$

where $F=-i(\delta-(|\Omega_1|^2-|\Omega_0|^2)/(h-\Delta))+\Gamma$. We can simplify the RHS of this equation considerably. Note that Bloch equations for the population difference found combining equations Eqs. (12) and (13)

$$\dot{\rho}_{aa}=i\tilde{\Omega}_1^*\rho_{ca}+c.c.+i\Omega_0^*\rho_{ac'}+c.c.+\frac{\gamma}{2}\rho_{cc}+\Gamma_1(\rho_{bb}-\rho_{aa}), \quad (12)$$

$$\dot{\rho}_{bb}=i\Omega_1\rho_{bc'}+cc.-i\Omega_2^*\rho_{cb}+cc.+\frac{\gamma}{2}\rho_{cc}-\Gamma_1(\rho_{bb}-\rho_{aa}), \quad (13)$$

indicate that in leading order, d is effectively a constant over the small range δ. Working to the leading order in Ω_2, the Bloch equation for ρ_{ca},

$$\dot{\rho}_{ca}=(-i(E-h)-\gamma_2)\rho_{ca}+i\tilde{\Omega}_1(\rho_{cc}-\rho_{aa})+i\Omega_0^*\rho_{cc'}-i\Omega_2\rho_{b\alpha}, \quad (14)$$

simplifies so that determining ρ_{ab} from Eq. (11) we may drop all Ω_2 dependent terms in ρ_{ac}, so that in steady state

$$(i\Delta+\gamma_2)\rho_{ac}=\frac{i}{2}\tilde{\Omega}_1(1+2d). \quad (15)$$

The same approximation for the Bloch equation for ρ_{cb},

$$\dot{\rho}_{cb}=(-iE-\gamma_2)\rho_{cb}+i\Omega_2(\rho_{cc}-\rho_{bb})-i\tilde{\Omega}_1\rho_{ab}+i\Omega_1\rho_{cc'}, \quad (16)$$

is a bit more complicated, in a steady state, so the leading order in Ω_2 reduces to

$$\left(i\Delta-\gamma_2-\frac{|\Omega_1|^2}{F}\right)\rho_{cb}=\frac{\Omega_1\Omega_0\tilde{\Omega}_1 d}{(h-\Delta)F}+i\Omega_2\left[-\frac{|\tilde{\Omega}_1|^2}{2F(i\Delta+\gamma_2)}(1+2d)+\left(\frac{1}{2}-d\right)\right], \quad (17)$$

and so, as indicated in the optical response in the Ω_1 field, Eq. (10), the main part of the δ (two-photon detuning) dependence is from the imaginary part of the ground-state coherence, ρ_{ab}. Thus, using Eqs. (15) and (17) in Eq. (11) and taking for simplicity that $\Omega_1=\tilde{\Omega}_1$ we simplify this in the small Ω_2 limit to

$$\rho_{ab}=\frac{i\Omega_1\Omega_0 d/(h-\Delta)+2\Omega_1\Omega_2(\gamma_2-i2\Delta d)/(\Delta^2+\gamma_2^2)}{i\left(\delta-\frac{|\Omega_1|^2-|\Omega_0|^2}{h-\Delta}\right)-\Gamma_2+\frac{|\Omega_1|^2}{i\Delta-\gamma_2}}, \quad (18)$$

which leads to a skew Lorentzian in the two-photon detuning δ of the optical response Eq. (10),

$$\text{Signal}\sim\frac{2\bar{\Gamma}\left(\frac{\Omega_1\Omega_0}{h-\Delta}-\frac{4\Omega_1\Omega_2\Delta}{\Delta^2+\gamma_2^2}\right)d-\frac{4\Omega_1\gamma_2}{\Delta^2+\gamma_2^2}\Omega_2\bar{\delta}}{\bar{\delta}^2+\bar{\Gamma}^2}, \quad (19)$$

where we have defined the offset two-photon detuning $\bar{\delta}=\delta-(|\Omega_1^2|-|\Omega_0|^2)/(h-\Delta)-|\Omega_1|^2\Delta/(\Delta^2+\gamma_2^2)$ and also the power broadened width $\bar{\Gamma}=\Gamma_2+|\Omega_1|^2\gamma_2/(\Delta^2+\gamma_2^2)$. This power broadening of the two-photon line shape is quite

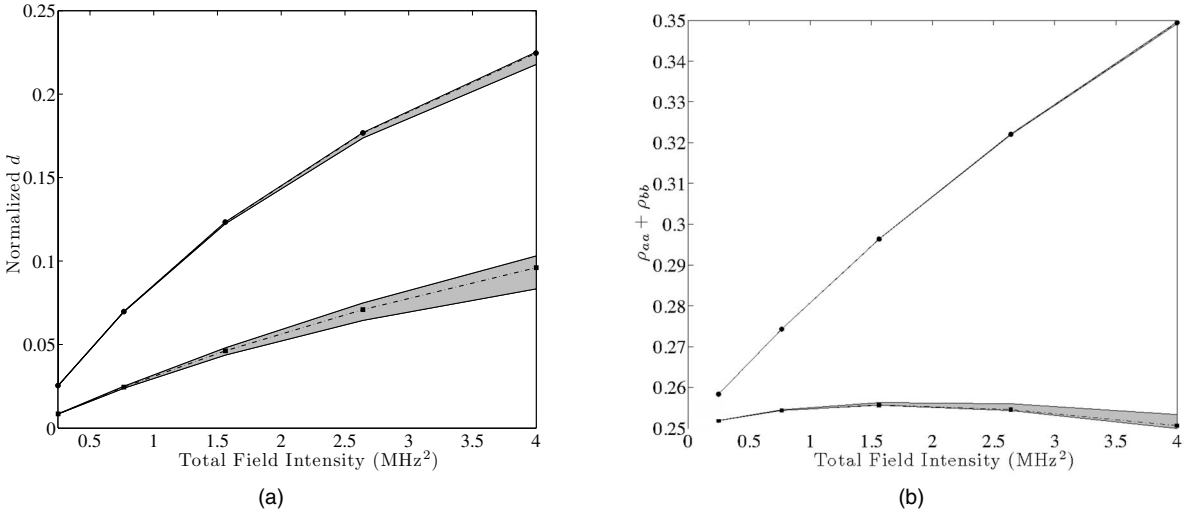

Fig. 4. Simulations of the $m=0$ clock transition N+CPT resonance on the D_1 and D_2 lines of ^{87}Rb. These plots are obtained by solving the truncated Floquet expansion to the second order in Ω_0, Ω_1, and Ω_2, using all 16 (resp. 24) states involved with the D_1 (resp. D_2) transitions. The axial magnetic field is $\vec{B}=100\,\hat{z}$ mG. For both plots, the upper curve (circles) for (a), the ground-state population difference or (b), the total population ($m=0$ states) (b) for the N+CPT system on the D_2 line while the lower curves (squares) result from N+CPT on the D_1 transition. The shaded area surrounding each curve indicates the range of variation of these parameters over a scan of the N+CPT resonance.

pronounced in experiments and typically dominates the natural ground-state width Γ_2.

Our model's predictions for the two-photon line asymmetry are discussed in [26]. The line asymmetry is defined as the ratio B/A of the symmetric and antisymmetric amplitudes of the skew Lorentzian [31,32],

$$\text{Signal} \sim \frac{A\Gamma + B\delta}{\delta^2 + \Gamma^2}. \tag{20}$$

The physical basis for the utility of the parametrization Eq. (20) is primarily a consequence of differential as

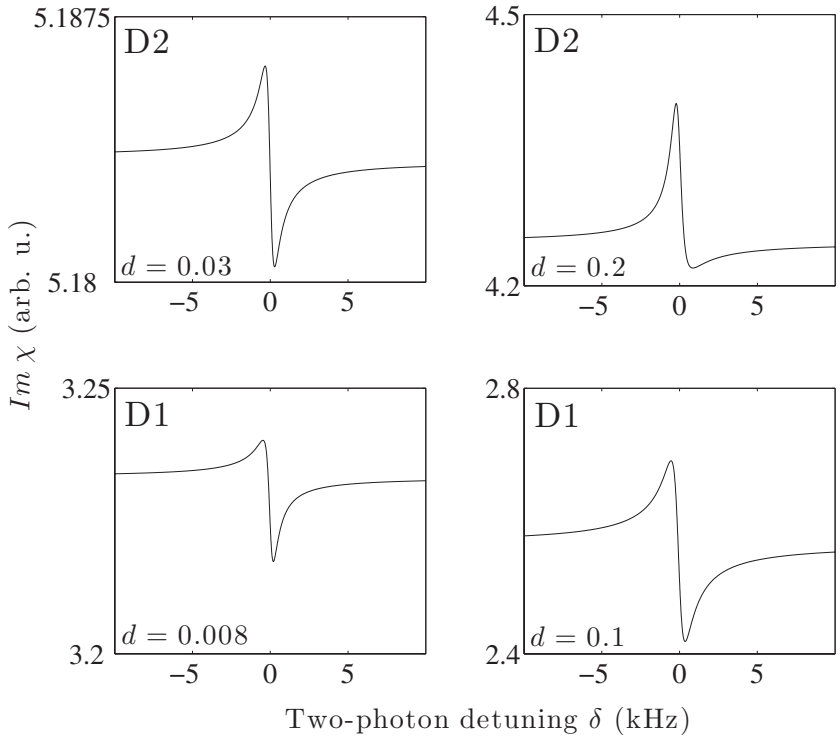

Fig. 5. Numerically calculated N+CPT lineshapes corresponding to the low and high power limits of Fig. 4 for the D_1 and the D_2 transitions. Line asymmetry decreases with increasing d, consistent with Eq. (19). Note that differences between the level structures of the $5\,^2P_{1/2}$ and $5\,^2P_{3/2}$ manifolds cause the D_2 N+CPT resonances to have less asymmetry for a given d than resonances on the D_1 line, due in large part to the relative enhancement of the D_1 CPT resonance. For small d on the D_1 line, the CPT transmission resonance actually dominates the N absorption peak.

Stark shifts as described for example in [26]. From Eq. (19) one sees that the asymmetry of this (two-photon) resonance is proportional to Ω_2 and inversely proportional to the ground-state population difference d. Although several approximations were used to derive Eq. (19), it does qualitatively reproduce much of the experimental phenomenology, such as the dependence on the amplitude (and not intensity) of the Ω_2 field and the fact that at larger optical power (but at fixed Ω_2/Ω_0 ratio) the ground-state population difference d is increased thus reducing the line asymmetry. Note that the approximations used to arrive at Eq. (19) include ignoring ac Stark effects in Ω_1 and Ω_0, and so one should not take that equation to strictly imply that in the $\Omega_2=0$ (pure N-resonance) limit the resonance becomes exactly symmetric. This interpretation of the experimental results is further supported by our numerical simulations (using TFS) of $N+$CPT resonances on the D_1 and D_2 lines of ^{87}Rb displayed in Fig. 4. In Fig. 4(a), we see that d for the D_2 line $N+$CPT resonance is significantly larger than that on the D_1 transition and that the variation of d [that we ignored in deriving Eq. (19)] as the field's frequencies sweep through resonance is also significantly smaller. The overall fraction of atoms populating the clock transition is also greater [Fig. 4(b)], owing in part to the smaller excited-state hyperfine splittings of the $5\,^2P_{3/2}$ manifold and to the absence of the $5\,^2P_{1/2}$, $F=2$, $m=2$ trap state for σ^+ light on the D_1 line.

Controlling the Rabi frequencies of the applied fields, we replicate the experimental observation that in typical buffer-gas vapor cells, using fields derived from a single modulated laser, D_2 line $N+$CPT resonances on the clock transition are more symmetric and have higher contrast than those on the D_1 line. We find the computed relationship between line asymmetry and optical pumping parameter d is also (Fig. 5) consistent with Eq. (19). To do that calculation the TFS was used to solve the full 16 (resp. 24) level system for an idealized two-field $N+$CPT resonance on the D_1 (resp. D_2) lines of ^{87}Rb, in the presence of an axial magnetic field of 100 mG. Furthermore, all terms that appear at the second order or lower in either the drive Ω_0, probe Ω_1, and CPT Ω_2 fields have been included.

The form of Eq. (19) also indicates that the peak of the optical response shifted. Working in the typical experimental regime, where the two-photon resonance width is power broadened, we find from Eq. (19) the location δ_* of the two-photon resonance peak

$$\delta_* = \frac{|\Omega_1|^2 - |\Omega_0|^2}{h-\Delta} + \frac{|\Omega_1|^2\Delta}{\Delta^2+\gamma_2^2} - \frac{4\Omega_2|\Omega_1|^2\gamma_2^2(h-\Delta)}{\Omega_0(\Delta^2+\gamma_2^2)^2}. \quad (21)$$

We now use this expression to locate the optimally stable operating regime for the joint resonance-based clock. In the $h \gg \Delta$ limit, one can locate a detuning compensation point, $\partial\delta_*/\partial\Delta|_{\Delta_{op}}=0$, at which the resonance peak's location will be insensitive (in leading order) to drifts in the laser's frequency. This gives an optimal one-photon detuning

$$\Delta_{op} = \gamma_2 + \frac{4\Omega_2 h}{\Omega_0}. \quad (22)$$

Further assuming operation at or near this Δ_{op}, we use Eq. (21) to find a light shift compensation condition. This condition is a sideband ratio at which the shift in the location of the peak in the two-photon joint resonance will be insensitive (to a leading order) to changes in the overall intensity of the laser. Substituting Eq. (22) into Eq. (21), assuming again that $h>\Delta$ keeping terms linear in Ω_2 we arrive at

$$\Delta_* = -\frac{\Omega_0^2}{2\gamma_2}\left[\frac{2\gamma_2}{h} - \frac{\Omega_1^2}{\Omega_0^2} + \frac{2h}{\gamma_2}\frac{\Omega_1^2\Omega_2}{\Omega_0^3}\right]. \quad (23)$$

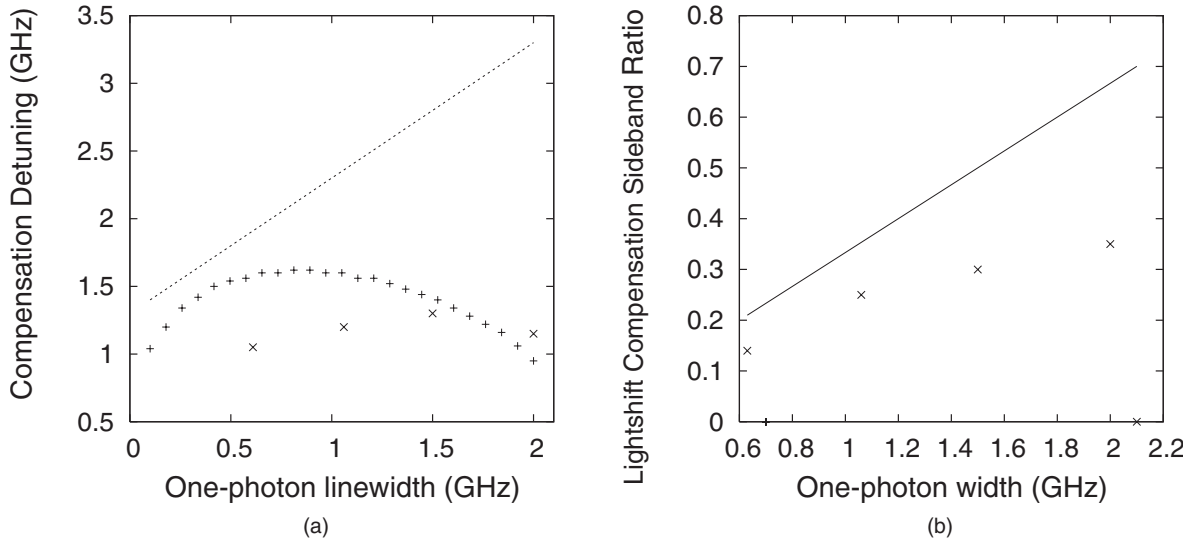

Fig. 6. (a) Detuning compensation frequency as a function of the one-photon line width. The "Xs" are for the analytical theory (which includes Boltzmann and Lamb–Dicke convolution), the "+s" are using a four-level TFS, and the dashed curve is a plot of Eq. (22). The fast modulation index was taken to be 0.6 and for the analytical theory the one-photon linewidth was computed in terms of the buffer-gas pressure. (b) Light shift cancellation Rabi ratio as a function of the one-photon linewidth. The Xs are, again, the analytical model evaluated however at the detuning compensation point (for each X) of the graph in part (a). For simplicity we have taken $\Omega_2=0$ in graph (b). The dashed line in (b) is from setting the RHS of Eq. (23) to zero.

The light shift compensation operating point is the sideband ratio at which the square bracket is zero. The Ω_2 term in that expression can make it more difficult to tune the fast modulation index of the current injected laser to reach this light shift compensation point.

Historically the importance of this operating point in one-photon detuning of Eqs. (22) and (23), light shift cancellation conditions were first pointed out by Tiachenachev and Yudin [24], and the weight of experimental evidence currently strongly supports the existence and robustness of this operating point for an N-resonance-based clock [19,20]. As a comparison with the complete theory model in Fig. 6 indicates, both of the approximate equations, Eqs. (22) and Eq. (23), apparently receive $\mathcal{O}(1)$ corrections as a consequence of additional effects from the inclusion of the c' level and ac Stark effects in the carrier Ω_0 and sideband Ω_1 field.

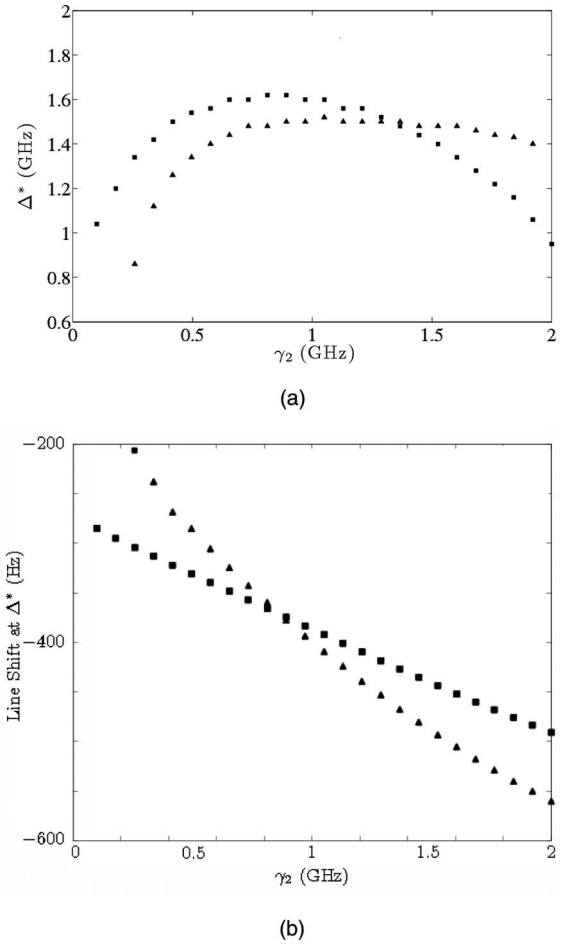

Fig. 7. (a) Plot of the one-photon detuning compensation point versus one-photon linewidth for the N+CPT resonance peak (squares) as well as the clock lock frequency (triangles) for a clock with slow modulation frequency 100 Hz with a slow modulation index of 0.6. In general, the compensation point for the absorption peak is different for that of the clock resonance as the N+CPT line asymmetry varies with one-photon detuning. At the intersection of the two curves in (a), the asymmetry is locally stable to variations in Δ. (b) Plot of the two-photon resonance shift (from h) of the absorption peak (squares) and clock resonance (triangles) versus one-photon linewidth for the same parameters at the one-photon detuning compensation point from (a).

We also performed a separate calculation of the N+CPT resonance using TFS but including only states directly involved with the N+CPT resonance clock transition, that is, the $F=1$, $m=0$, and $F=2$, $m=0$ $5\,^2S_{1/2}$ ground states, and the $F=1$, $m=1$, and $F=2$, $m=1$ $5\,^2P_{1/2}$ excited states. In doing so, we calculate the response of this four-level system to the five strongest fast modulation sidebands in the presence of additional slow modulation sidebands, using 15 fields coupled to all four optical transitions to directly simulate the error signal for a modulated N+CPT resonance clock. All terms that are second order in any of the five fast modulation sidebands or the first order in any pair of fast modulation sidebands are included, as are any terms that are first order in the ten slow modulation sidebands. A graphical representation of the unconstrained equations of motion is displayed in Fig. 3 showing the size of the resulting system of equations. This model allows us to directly simulate the operation of a typical clock, where the phase of the amplitude modulated beatnote resulting from the slow modulation sidebands interaction with the resonance provides an error signal for stabilizing the clock frequency. The zero crossing of this beatnote, and not necessarily the position of the absorption peak, is the clock lock frequency. Using the TFS model, we have computed both the two-photon light shift and the optimal Δ_* for the clock lock point as well as for the two-photon resonance peak as a function of the one-photon linewidth shown in Fig. 7. For a fixed line asymmetry, the optimal one-photon detuning should be the same for both the peak and the lock point. Instead, the clock resonance is generally stable for Δ's, which do not provide stability for the peak absorption and vice versa. Points at which both the clock resonance and the absorption peak position are stable for the same Δ correspond to points at which the asymmetry is stable to variations of Δ. Searches for stable operating points of clocks based upon asymmetric resonances must in general include a study of how the slow modulation parameters affect the clock frequency shift (see also [14,15] in the CPT case).

5. CONCLUSION

We have described and solved a quantum optics model for the properties of a Λ system in light fields that excite both a CPT and an N-resonance. By incorporating all the leading order ac Stark effects of a five-sideband modulation comb, we have derived an analytical expression explaining the properties of the joint N+CPT resonance. Further, we have developed the OBE to a higher order in the optical fields and couplings using a computer symbolic manipulation and evaluation program using TFS. Both of these approaches reveal profound sensitivity of the resonance shape to the modulation parameters of the applied fields as well as the importance of optical pumping on the lineshape asymmetry. Both of our theoretical approaches agree semi-quantitatively with previous experiments with regard to power broadening and line asymmetry in addition to light shifts and their dependence upon one-photon detuning. The model we have developed will be an invaluable aid in the optimization of emerging clock designs using current modulated laser diodes, including

miniature atomic clocks. In particular, the differences that we have noted in the behavior of the absorption resonance shift as compared to that of the lock point (clock resonance) of such a clock suggest that the slow modulation parameters may also contribute to the overall optimization.

ACKNOWLEDGMENTS

This work was supported by the Office of Naval Research (ONR) and in part by the National Science Foundation (NSF) through a grant to the Institute of Theoretical Atomic and Molecular Physics at Harvard University and the Smithsonian Astrophysical Observatory, and the Research Professorship Program through Youngstown State University. We also acknowledge support from the Radcliffe Institute for Advanced Studies, where this work was completed.

REFERENCES

1. E. Arimondo, "Coherent population trapping in laser spectroscopy," in *Progress in Optices XXXV*, E. Wolf, ed. (Elsevier, 1996), p. 257.
2. J. Vanier, M. W. Levine, D. Janssen, and M. J. Delaney, "On the use of intensity optical pumping and coherent population trapping techniques in the implementation of atomic frequency standards," IEEE Trans. Instrum. Meas. **52**, 822–831 (2003).
3. J. Kitching, S. Knappe, N. Vukičeviè, L. Hollberg, R. Wynands, and W. Weidmann, "A microwave frequency reference based on VCSEL-driven dark line resonances in Cs vapor," IEEE Trans. Instrum. Meas. **49**, 1313–1317 (2000).
4. S. Knappe, R. Wynands, J. Kitching, H. G. Robinson, and L. Hollberg, "Characterization of coherent population-trapping resonances as atomic frequency references," J. Opt. Soc. Am. B **18**, 1545–1553 (2001).
5. M. Merimaa, T. Lindvall, I. Tittonen, and E. Ikonen, "All-optical atomic clock based on coherent population trapping in ^{85}Rb," J. Opt. Soc. Am. B **20**, 273–279 (2003).
6. L. A. Liew, S. Knappe, J. Moreland, H. Robinson, L. Hollberg, and J. Kitching, "Microfabricated alkali atom vapor cells," Appl. Phys. Lett. **84**, 2694–2696 (2004).
7. S. Knappe, V. Shah, R. Wynands, P. D. D. Schwindt, L. Hollberg, J. Kitching, L. A. Liew, and J. Moreland, "A microfabricated atomic clock," Appl. Phys. Lett. **85**, 1460–1462 (2004).
8. J. Kitching, H. G. Robinson, L. Hollberg, S. Knappe, and R. Wynands, "Optical-pumping noise in laser-pumped, all-optical microwave frequency references," J. Opt. Soc. Am. B **18**, 1676–1682 (2001).
9. R. Lutwak, D. Emmons, W. Riley, and R. M. Garvey, "The chip-scale atomic clock and coherent population trapping vs. conventional interrogation," in *34th Annual Precise Time and Time Interval (PTTI) Meeting*, 539–550 (Naval Observatory, 2002).
10. J. C. Comparo and J. G. Coffer, "Conversion of laser phase noise to amplitude noise in a resonant atomic vapor: the role of laser linewidth," Phys. Rev. A **59**, 728–735 (1999).
11. J. G. Coffer and J. C. Comparo, "Diode laser linewidth and phase noise to intensity noise conversion in a gas-cell atomic clock," in *Proceedings of IEEE International Frequency Control Symposium (I.F.C.S.)* (IEEE, 1998), (1998), pp. 52–56.
12. J. C. Comparo, "Conversion of laser phase noise to amplitude noise in an optically thick vapor," J. Opt. Soc. Am. B **15**, 1117–1186 (1998).
13. F. Levi, A. Godone, and J. Vanier, "Light shift effects in the coherent population trapped cesium maser," IEEE Trans. Ultrason. Ferroelectr. Freq. Control **47**, 466–470 (2000).
14. A. de Marchi, G. D. Rovera, and A. Premoli, "Effects of servo loop modulation in atomic beam frequency standards employing a Ramsey cavity," IEEE Trans. Ultrason. Ferroelectr. Freq. Control **34**, 582–591 (1987).
15. D. F. Phillips, I. Novikova, C. Wang, M. Crescimanno, and R. L. Walsworth, "Modulation induced frequency shifts in a CPT-based atomic clock," J. Opt. Soc. Am. B **22**, 305–310 (2005).
16. M. Zhu and L. S. Cutler, "Theoretical and experimental study of light shift in CPT-based Rb vapor cell frequency standard," in *32nd Ann. Precise Time and Time Interval (PTTI)*, 311–324 (Naval Observatory, 2000).
17. J. Vanier, "Atomic clocks based on coherent population trapping: a review," Appl. Phys. B **81**, 421–442 (2005).
18. A. S. Zibrov, C. Y. Ye, Y. V. Rostovtsev, A. B. Matsko, and M. O. Scully, "Observation of a three-photon electromagnetically induced transparency in hot atomic vapor," Phys. Rev. A **65**, 043817 (2002).
19. S. Zibrov, I. Novikova, D. F. Phillips, A. V. Taichenachev, V. I. Yudin, R. L. Walsworth, and A. S. Zibrov, "Three photon absorption resonance for all-optical atomic clocks," Phys. Rev. A **72**, 011801(R) (2005).
20. S. Zibrov, I. Novikova, D. F. Phillips, A. V. Taichenachev, V. I. Yudin, R. L. Walsworth, and A. S. Zibrov, "A novel absorption resonance for atomic clocks," in *Proceedings of the 2005 Joint IEEE International Frequency Control Symposium and Precise Time and Time Interval (PTTI) Systems and Applications Meeting* (IEEE, 2005), p. 767.
21. I. Novikova, D. F. Phillips, A. S. Zibrov, R. L. Walsworth, A. V. Taichenachev, and V. I. Yudin, "Cancellation of light shifts in an *N*-resonance clock," Opt. Lett. **31**, 622–624 (2006).
22. I. Novikova, College of William and Mary (personal communication, March, 2008).
23. I. Novikova, D. F. Phillips, A. S. Zibrov, R. L. Walsworth, A. V. Taichenachev, and V. I. Yudin, "Comparison of ^{87}Rb *N*-resonances for D_1 and D_2 transitions," Opt. Lett. **31**, 2353–2355 (2006).
24. A. V. Taichenachev and V. I. Yudin, Laser Physics Laboratory, Novosirsk State University (personal communication, May, 2005).
25. Y. Xiao, I. Novikova, D. F. Phillips, and R. L. Walsworth, "Diffusion induced Ramsey narrowing," Phys. Rev. Lett. **96**, 043601 (2006).
26. C. Hancox, M. Hohensee, M. Crescimanno, D. F. Phillips, and R. L. Walsworth, "Lineshape asymmetry in joint CPT- and *N*-double resonance," Opt. Lett. **33**, 1536–1538 (2008).
27. J. H. Shirley, "Solution of the Schroedinger equation with a Hamiltonian periodic in time," Phys. Rev. **138**, B979–B987 (1965).
28. D. I. Duncan, J. G. Story, and T. F. Gallagher, "Floquet description of multiphoton processes in Li," Phys. Rev. A **52**, 2209–2217 (1995).
29. A. Emmanouilidou and L. E. Reichl, "Floquet scattering and classical-quantum correspondence in strong time-periodic fields," Phys. Rev. A **65**, 033405 (2002).
30. B. H. Wu and J. C. Cao, "A Floquet–Green's function approach to mesoscopic transport under ac bias," J. Phys.: Condens. Matter **20**, 085224 (2008).
31. S. Knappe, M. Stähler, C. Affolderbach, A. V. Taĭchenachev, V. I. Yudin, and R. Wynands, "Simple parametrization of dark-resonance line shapes," Appl. Phys. B **76**, 57–63 (2003).
32. A. V. Taĭchenachev, V. I. Yudin, R. Wynands, M. Stähler, J. Kitching, and L. Hollberg, "Theory of dark resonances for alkali-metal vapors in a buffer-gas cell," Phys. Rev. A **67**, 033810 (2003).